

Free-Stream Turbulence Effects on Leading Edge Film Cooling

Ken-ichi Funazaki¹, Hirokazu Kawabata² and Yoji Okita³

¹ Department of Mechanical Engineering
Iwate University

3-5 Ueda, Morioka-shi, Iwate 020-8551, JAPAN

² Graduate School of Mechanical Engineering, Iwate University

³ IHI Corporation

ABSTRACT

This study deals with the experimental and numerical studies of the effect of free-stream turbulence on turbine blade leading edge film cooling. The study examines several test cases with two blowing ratios (BR=1.0 and 2.0) and three mainstream turbulence intensities (1.0, 3.3 and 12.0 %) using two types of leading edge models with cylindrical holes and diffuser holes [1]. The leading edge model consists of a semi-circular part of 80mm diameter and a flat after-body. Film effectiveness and heat transfer coefficient on the model surface are measured by the transient method using thermochromatic liquid crystal with video camera. In addition, detailed investigation of the film cooling is carried out using CFD simulations. RANS approach using Shear Stress Transport turbulence model was employed to solve the flow field. In the case of diffuser hole, the effect of mainstream turbulence intensity appears significantly, and spanwise averaged film effectiveness is decreased.

NOMENCLATURE

BR	: Blowing ratio
C_p	: Pressure coefficient
D	: Diameter of the leading edge model, mm
d	: Diameter of film cooling holes, mm
FP	: Flat plate geometry region
h	: Heat transfer coefficient, W/(m ² K)
P	: Pressure, Pa
Re_D	: Reynolds number
SC	: Semi-circular geometry region
T	: Temperature, K
TLC	: Thermochromatic liquid crystal
Tu	: Turbulence intensity
t	: Time, s
U	: Main stream velocity, m/s
x, y, z	: Cartesian coordinates, mm
α	: Angle, deg
η	: Film cooling effectiveness
μ	: Viscosity, Pa s
ρ	: Density, kg/m ³

Subscripts

aw	: Adiabatic wall
------	------------------

ave	: Average in the spanwise direction of the model
d	: Dynamic quantity
f	: Fluid
m	: Relative to mainstream
L	: Leading edge surface
t	: Stagnation
w	: Wall
2	: Relative to secondary air

INTRODUCTION

In order to raise thermal efficiency of a gas turbine, higher turbine inlet temperature (TIT) is needed. However, higher TIT increases thermal load to its hot-section components and reducing their life span. Therefore, very complicated cooling technology such as film cooling and internal cooling is required especially for HP turbine blades. In film cooling, relatively cool air is injected onto the blade surface to form a protective layer between the surface and hot mainstream gas. The highest thermal load usually occurs at the leading edge of the airfoil, and failure is likely to happen in this region. Film cooling is typically applied to the leading edge through an array of hole rows called showerhead. The flow near the leading edge is extremely complicated with stagnation, strong pressure gradients and curvature, and interaction between mainstream and coolant jets become increasingly complex, which implies the difficulty of proper cooling around this area. Therefore, increases in film effectiveness in the leading edge will lead to significant benefits in life and efficiency of the turbine blade.

Mehendale and Han [2] used a blunt body with a semi-circular leading edge and a flat afterbody to study the effect of high mainstream turbulence on leading edge film cooling and heat transfer. Two turbulence level ($Tu = 9.67$ percent and $Tu = 12.9$ percent) were generated by passive grid and a jet grid at a leading edge Reynolds number of 100,000. Film coolant was injected through two rows of film holes at ± 15 and ± 40 degrees from the stagnation with three blowing ratios of 0.4, 0.8, and 1.2. They found that the leading edge film effectiveness for a blowing ratio of 0.4 was significantly reduced by high mainstream turbulence. For blowing ratio of 0.8 and 1.2 the mainstream turbulence effect was diminished in the leading edge but still existed on the flat sidewall region. They also pointed out that the leading edge heat transfer coefficient for blowing ratio of 0.8 increased with mainstream turbulence, but the effect was not consistent for blowing ratio of 0.4 and 1.2. Ekkad et al. [3] studied the effect of free stream turbulence on the detailed distributions of film effectiveness and heat transfer coefficient on a cylindrical leading edge model using transient liquid crystal image method.

Their results also show that higher mainstream turbulence reduces the film effectiveness for lower blowing ratios but the effect diminishes at higher blowing ratio. Rozati et al. [4-5] and Takahashi et al. [6] studied leading edge film cooling by numerical method with Large Eddy Simulation and Detached-Eddy Simulation. Although they compared the numerical aerothermal performance with the experiment results, the effect of free stream turbulence was not taken into account in their simulation.

Saumweber et al. [7] studied free stream turbulence effect on flat plate film cooling with shaped holes. They found that the effect of increased turbulence level is detrimental to film effectiveness of the shaped hole at all blowing ratios. Laterally averaged film effectiveness is reduced up by 30% when the turbulence intensity is increased from 3.6 to 11%. The effect is more pronounced at smaller blowing ratios. Kim et al.[8] and Reiss et al.[9] studied the influence of shaped injection holes on leading edge film cooling. They found that the holes with laid-back-type widened exits clearly enhanced the overall cooling performance of the showerhead, compared to classical cylindrical hole cases. However, the effect of free stream turbulence was not investigated in these studies. York et al. [10] used a computational methodology for the analysis of film cooling from diffused holes on the simulated leading edge of a turbine airfoil. Their results show that the advantage in effectiveness was due to the shallower trajectory of the coolant exiting the holes, causing it to stay closer to the surface than in the case of nondiffused holes. But, there were few examples which studied the effect of cooling hole shape and mainstream turbulence.

In this investigation, the influences of hole shape as well as free stream turbulence on leading edge film cooling are studied. The objective of the present study is to investigate the effects of free stream turbulence on the leading edge film cooling from cylindrical holes and diffuser holes using the experimental and numerical techniques. Three turbulence levels and four blowing ratios are investigated and the result of heat transfer coefficient and the film cooling effectiveness are reported.

EXPERIMENT

Experimental Facility

Figure 1 shows the test apparatus. The experiment was conducted by the wind tunnel for heat transfer test at Iwate University. Two air supply systems exist in the experimental facility, and secondary air is heated with a heater. Secondary air was supplied to the test model installed in the center of the test section duct from upper piping. The mainstream velocity was measured by a Pitot tube installed 210mm upstream of the stagnation point of the test model. The test section duct was built with acrylics plates, the cross-section areas of test section were 280mm×450mm, and length was 1150mm (360mm from the stagnation point of test model to a test section duct entrance). The static pressure holes were prepared by both side of the test model on the lower plate of the test duct to check the symmetric flow around the model with respect to the duct center line. In this study, the difference of static pressure on either side was adjusted so as to be less than 1Pa. Two types of turbulence grid (Grid A, Grid B) were attached to the inlet of the transition duct. The distance from stagnation point of test model to turbulence grid was 750mm. Grid A consisted of stainless steel pipe 8mm in diameter. Grid B was composed of square wooden of bars(12mm×12mm). When measuring the mainstream turbulence intensity, I-type hot wire anemometer was used along with DANTEC Stream Line System. SONY DCR-VX2000 CCD camcorder used for recording TLC painted test model surface was installed in the angle of 60° from the stagnation point of the test model.

In this study, the test model for static pressure measurement and two type of test model with film cooling holes were prepared. Figure 2(a) shows the test model for static pressure measurement. The test model has a semi-circular part of 80mm in diameter (D), and flat plate parts of 100mm in length, and the height of the test model is 280mm. In the heat transfer measurement, only one side of

the test model was monitored. On the flat plate area, a length of 9.36d (=75mm) was viewed. When installing the test model in test section, flat plate region was extended by 650mm in the streamwise direction with a acrylics plates. The hole for measuring static pressure was prepared in the mid-span of the test model. Any cooling holes were not prepared in this test model. Each of the static pressure holes was equally spaced by 10 degrees in the semi-circular region. Static pressure holes were also created on the flat plate region 8mm downstream of the junction between the semi-circular part and flat plates part.

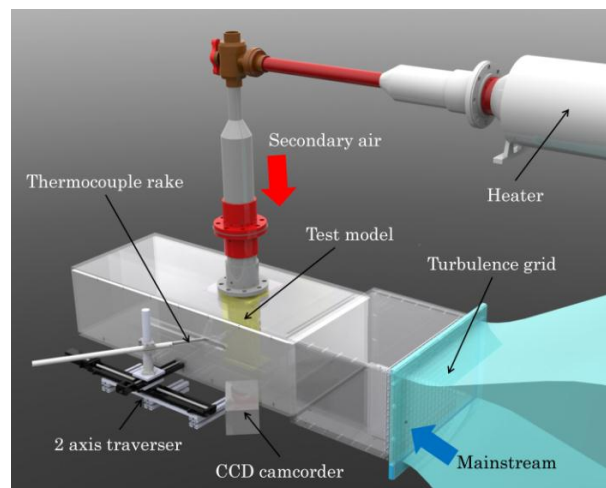
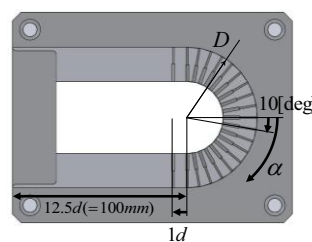
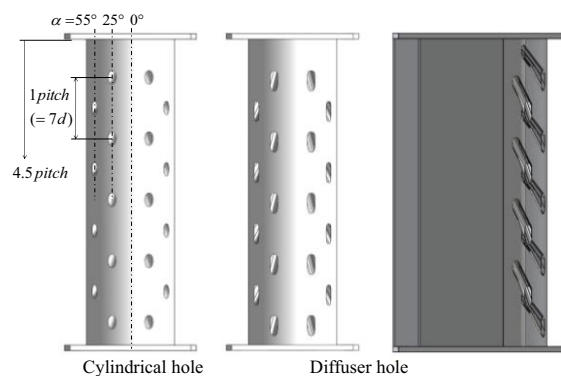
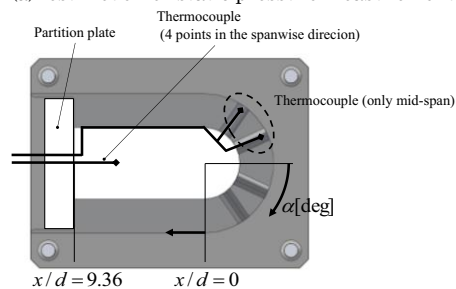


Fig.1 Experimental facility



(a) Test model for static pressure measurement



(b) Test model for heat transfer measurement

Fig.2 Test model : (a) model for pressure measurement and (b) model for heat transfer measurement

Figure 2(b) shows two types of test models that have film cooling holes for heat transfer measurement. Most of the dimensions of the test model with cooling holes were the same as those of the test model with static pressure holes. The shapes of film cooling hole exits were cylindrical and diffuser-shaped. The equivalent diameter of the cooling hole (d) was 8mm, and the diffuser cooling holes were expanded toward holes exit. The cooling hole was prepared in the position of $\alpha = \pm 25^\circ$ and $\alpha = \pm 55^\circ$ at each test model. However, only the region of $\alpha \geq 0^\circ$ was captured by CCD camera in heat transfer measurement. The angle of inclination of cooling hole to the surface was 40° . A partition plate for preventing secondary air from leaking outside was installed in the back section of plenum. Four holes were drilled in partition plate and it was possible to measure the temperature in plenum in the height direction at four places. Furthermore, the temperature in the cooling hole of mid-span was measured by two more thermocouples on the partition plate.

Test Conditions

All tests were conducted in the wind tunnel at Reynolds number of 43,000 based on leading edge diameter (D). Blowing ratios ($BR = \rho_c U_c / \rho_m U_m$) were examined 0.5, 1.0, 1.5 and 2.0. Figure 4 shows streamwise distributions of turbulence intensity measured at the mid span. These minimum turbulence intensities are referred to as the reference turbulence intensities in this study. Therefore, the reference turbulence intensity for the Grid A and Grid B are 3.3 and 12.0 percent, respectively.

In this study, since only the half of a test model was observed by CCD camera in the heat transfer measurement, it was necessary to check the symmetry of the flow in the test section. Therefore, the test model for static pressure measurement shown in Fig. 2(a) was used for the measurement of static pressure. The static pressure coefficient was calculated by

$$C_p = \frac{P_t - P_L}{P_d} \quad (1)$$

Here, total pressure and dynamic pressure were definition by Pitot tube positioned 210mm 210mm upstream of the stagnation point. Since wake generated by the Grid was expected to hit Pitot tube, it was moved to three different places to obtain each of time averaged values. The values of C_p at the test model in each test condition are shown in Figure 4. C_p distribution is almost symmetrical with respect to the stagnation line ($\alpha = 0^\circ$), indicating that the stagnation point did not shift even under the influence of free-stream turbulence. Although the separation appeared at $\alpha = 90^\circ$ in No Grid and Grid A case, it was no longer observed in Grid B case.

Theory of transient TLC technique

In this study the test model was coated with TLC (Nihon microcapsule). The nominal color bands of TLC was from 22.5°C to 30.5°C.

The present study used two different reference temperatures to determine film effectiveness and heat transfer coefficients both from a single test in a way proposed by Kim et al. [11].

When a semi-infinite substance of initial temperature T_i is exposed to a flow whose temperature $T(t)$ starts to increase at a certain instant, its surface temperature $T_w(t)$ accordingly rises. Suppose that heat transfer coefficient of the flow h is constant, $T_w(t)$ can be expressed by Eqs. (2) and (3) using Duhamel's theorem,

$$T_w(t) - T_i = \sum_{j=1}^N U(t - \tau_j)(T_j - T_{j-1}), \quad (2)$$

$$U(t - \tau_j) = 1 - \exp(\beta^2) \operatorname{erfc}(\beta), \quad \beta = \frac{h\sqrt{t - \tau_j}}{\sqrt{\rho c k}} \quad (3)$$

where the increase in the flow temperatures is approximated by a

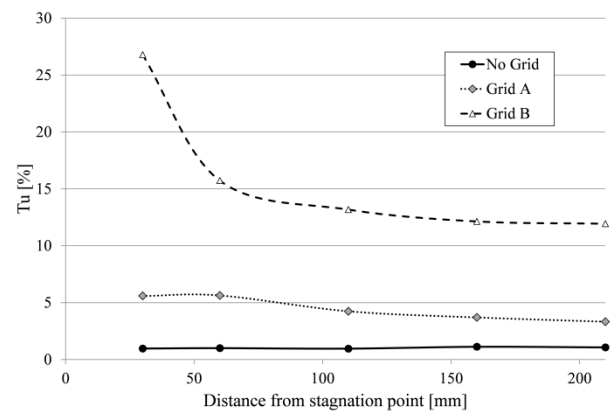


Fig.3 Streamwise distributions of turbulence intensity

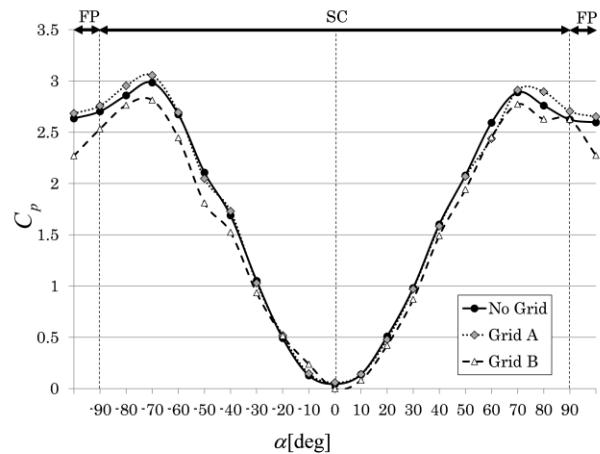


Fig.4 Static pressure distribution

summation of small temperature steps ($T_j - T_{j-1}$) with the time lag from the initiation τ_j , and $U(t - \tau_j)$ in Eq. (3) is an exact solution of the equation for the one-dimensional unsteady heat conduction under the abrupt increase in the flow temperature. Eq. (2) can yield the heat transfer coefficient h using the information on the temporal variation of the surface temperature as well as the temperature rise of the flow over the surface.

When a film cooling exists, its effect upon the flow temperature should be taken into account through the film cooling effectiveness η , which is defined as follows:

$$\eta = \frac{T_{aw} - T_\infty}{T_2 - T_\infty}, \quad (4)$$

where T_{aw} , T_∞ and T_2 are adiabatic wall temperature, primary flow temperature and secondary flow temperature, respectively. Using this relationship, along with the assumption that η is constant even when the secondary flow temperature varies with time, the temperature T_j in Eq. (2) can be replaced by the corresponding adiabatic wall temperature $T_{aw,j}$ given by

$$T_{aw,j} = \eta T_{2,j} + (1 - \eta) T_\infty \quad (5)$$

From this expression the following expression is obtained.

$$T_{aw,j} - T_{aw,j-1} = \eta(T_{2,j} - T_{2,j-1}) \quad (6)$$

Therefore, replacing $(T_j - T_{j-1})$ in Eq. (2) by $(T_{aw,j} - T_{aw,j-1})$, one can obtain the expression for the surface temperature,

$$T_w(t) - T_i = \eta \sum_{j=1}^N U(t - \tau_j)(T_{2,j} - T_{2,j-1}). \quad (7)$$

Use of the above expressions for different two instants $t = t_a$ and $t = t_b$ to eliminate η yields the following equation,

$$\frac{T_w(t_a) - T_i}{T_w(t_b) - T_i} = \frac{\sum_{j=1}^N U(t_a - \tau_j)(T_{2,j} - T_{2,j-1})}{\sum_{j=1}^N U(t_b - \tau_j)(T_{2,j} - T_{2,j-1})} \quad (8)$$

Then the heat transfer coefficient h can be determined from Eq. (8), using a proper method for solving non-linear equations. Substituting the resultant heat transfer coefficient into Eq. (7), film effectiveness is then calculated as follows,

$$\eta = \frac{T_w(t_a) - T_i}{\sum_{j=1}^N U(t_a - \tau_j)(T_{2,j} - T_{2,j-1})} \quad (9)$$

Temperature measurement around the model

In this study, a thermocouple rake was used to perform temperature measurement within planes normal to the test model surface. The thermocouple rake consists of 13 K-type thermocouples. These thermocouples were installed at 5mm pitch. Locations of the temperature measurement by this thermocouple rake are shown in Figure 5(a). Measurement planes are $\alpha = 40^\circ, 70^\circ, 90^\circ$ and $x/d = 9.36d$ (Flat plate position). Figure 5(b) shows the measurement grid. 50 points temperature measurement was performed in the direction of normal to model surface at 1mm intervals. Measurement planes were located in mid-span of the test model. The non-dimension temperature is similarly defined as film effectiveness, and it is calculated by following Eq. (10).

$$\eta = \frac{T_f - T_m}{T_2 - T_m} \quad (10)$$

where T_2 was the mean temperature of two thermo couples in the inside of cooling holes.

NUMERICAL SIMULATION

A commercial software, ANSYS CFX 12 was used in this study. Time-averaged Reynolds-Averaged Navier-Stokes (RANS) approach using Shear-Stress Transport (SST) two-equation model was employed. Figure 6 shows the computational domain simulating the experimental setups and the mesh. Because of the flow symmetry, the domain was restricted to the left half of the flow field around the test model. The height of the domain was $14d$, which was enough to cover 2pitch of test model. Although tetra mesh was mainly used for the computational grid, Prism mesh also was used in order to resolve boundary layer at near wall region. Total number of the cell was about 11,000,000 cells in this domain, where 9,000,000 cells were used for the test section duct region, and 2,000,000 cells were used for plenum and film holes region. The mainstream flow velocity measured in the experiment, temperature and turbulence intensity were specified at the mainstream entrance. The mass flow rate and temperature measured in the experiment were imposed at the secondary air entrance. The boundary condition of symmetry was used for the center of the computational domain.

RESULT AND DISCUSSION

Detailed experimental results of film cooling effectiveness and heat transfer coefficient distributions for cylindrical hole case are presented in Figure 7. Since the liquid crystal coating without the influence of the injected air did not change its color, the temperature data was not obtained in the black region in this figure. In $BR=1.0$ case, the film effectiveness distribution found from $\alpha = 55^\circ$ cooling hole expanded in the spanwise direction compared with film effectiveness distribution from $\alpha = 25^\circ$ cooling hole. The difference is due to static pressure distribution around the leading edge model and different blowing ratio of each film cooling hole. At $\alpha = 90^\circ$, the film effectiveness distribution expanded in the spanwise direction because the mainstream separated. When the

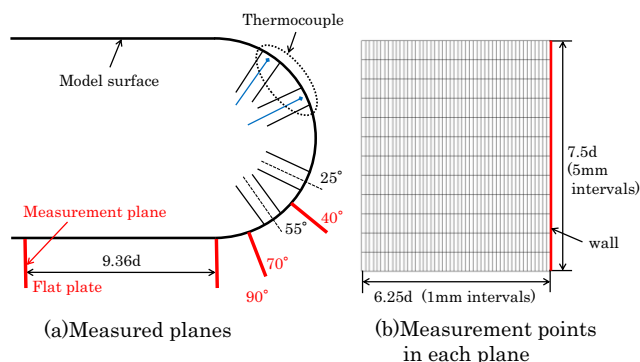


Fig.5 Measured planes and measurement grid (a)measured planes and (b)measurement grid

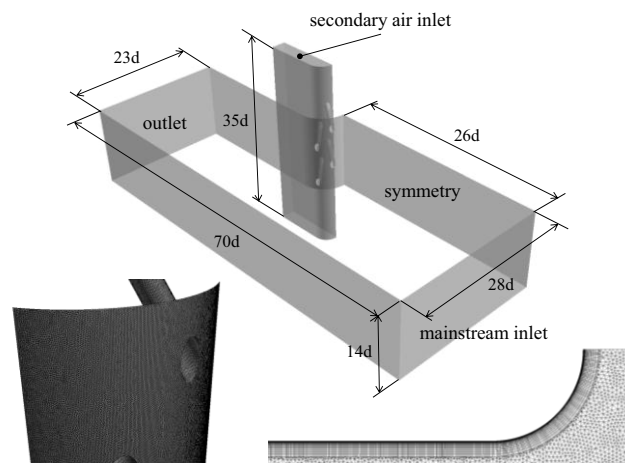


Fig.6 View of the computational domain and mesh

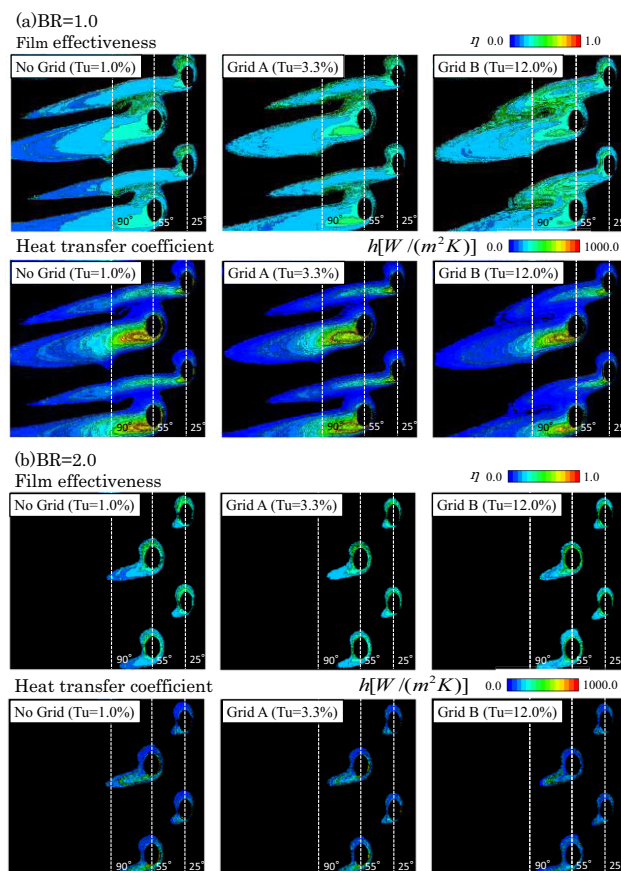


Fig.7 Film effectiveness and heat transfer coefficient for cylindrical hole (a)BR=1.0 and (b)BR=2.0

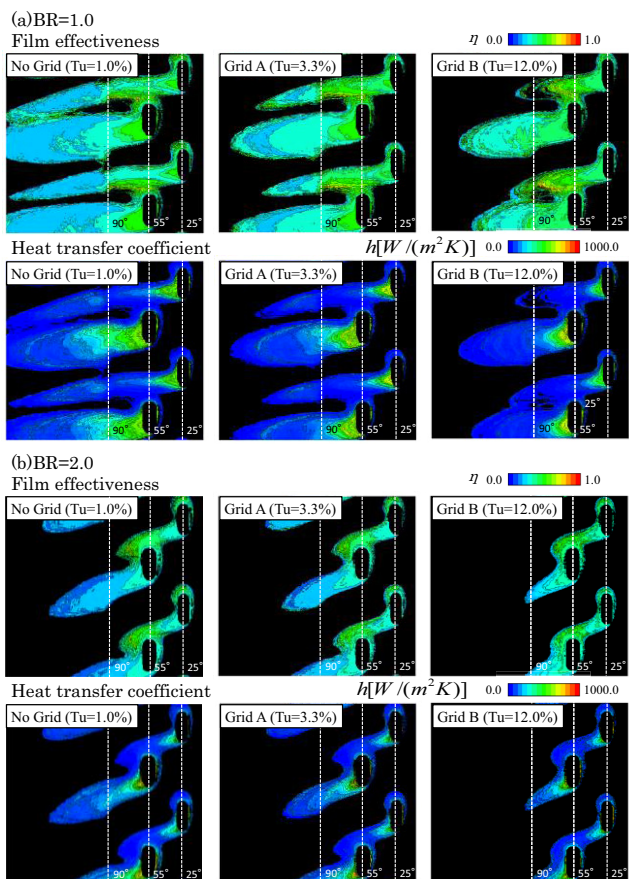


Fig.8 Film effectiveness and heat transfer coefficient for diffuser hole (a)BR=1.0 and (b)BR=2.0

mainstream turbulence intensity became high, any film effectiveness distribution expansion was not clearly observed in the downstream region from $\alpha=90^\circ$. Especially this tendency was remarkably observed to the film effectiveness distribution found from the $\alpha=25^\circ$ cooling hole. On the other hand, in semi-circular region, the film effectiveness reduction was hardly seen. In the case of Tu=12.0%, reduction of film effectiveness was observed by mainstream turbulence, but the secondary air which ejected from $\alpha=25^\circ$ cooling holes interfered with the secondary air ejected from $\alpha=55^\circ$ cooling holes, and the film effectiveness distribution expanded in the spanwise direction. In BR=2.0 case, since secondary air penetrated into the main flow, film effectiveness distribution was hardly seen. In addition, even if the mainstream turbulence intensity became high, reduction of film effectiveness as in BR=1.0 case was not seen. As for heat transfer coefficient, the heat transfer coefficient near cooling holes became high. Since the heat transfer coefficient can measure only the region where TLC color changes, it cannot be compared with numerical results completely.

Detailed experimental results of film cooling effectiveness and heat transfer coefficient distributions for diffuser hole case are presented in Figure 8. The expansion of film effectiveness is as large as in cylindrical hole case in BR=1.0 case. Compared with cylindrical hole case, film effectiveness distribution expanding was large in diffuser hole case. This can be explained by the effect of reduced momentum of the secondary air from the diffuser hole, which made the air attached to the test model surface. Film effectiveness distribution tended to expand in comparison with cylindrical hole case at BR=2.0 case. In diffuser hole BR=1.0 case, when the mainstream turbulence intensity increased, the expansion of the film effectiveness was no longer observed, but unlike cylindrical hole case, reduction of the film effectiveness distribution from $\alpha=55^\circ$ cooling holes was seen remarkably. Film effectiveness also decreased at BR=2.0 case more remarkably than cylindrical hole

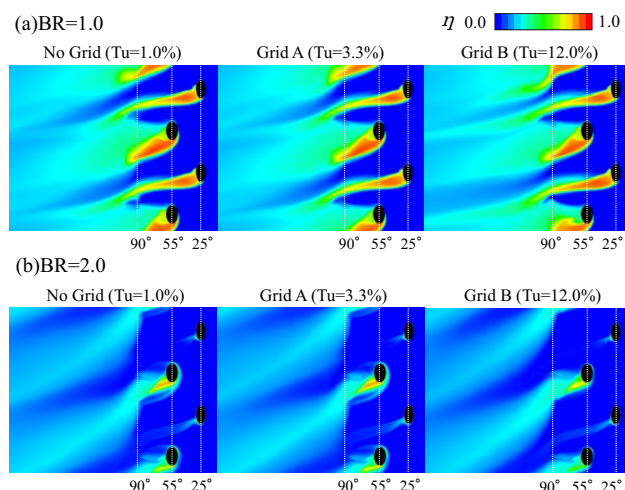


Fig.9 The contours of film cooling effectiveness for cylindrical hole (a)BR=1.0 and (b)BR=2.0

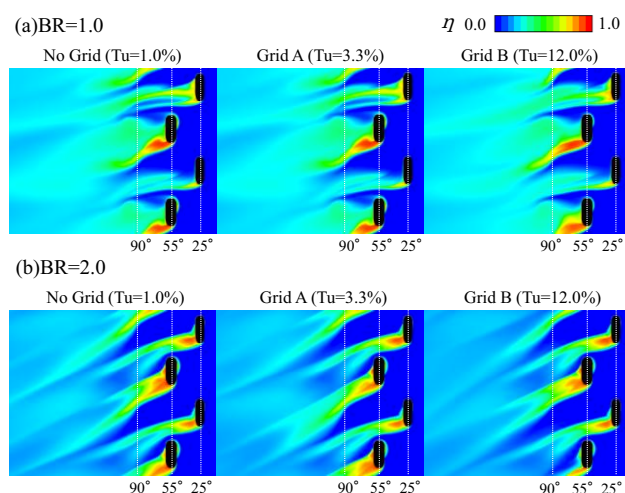


Fig.10 The contours of film cooling effectiveness for diffuser hole (a)BR=1.0 and (b)BR=2.0

case. Although the heat transfer coefficient was high near the cooling hole as in cylindrical hole case, in BR=1.0 case, the heat transfer coefficient near the cooling holes lower than cylindrical hole case.

Figure 9 shows the film effectiveness distribution of cylindrical hole case obtained by CFD. In the CFD result, the film effectiveness near the cooling holes was higher than the experimental result. In the case of BR=0.5 No Grid, the CFD result was qualitatively similar to the experimental result in semi-circular region, but in the flat plate region, the film effectiveness distribution expansion was overpredicted compared with the experimental result. Although $\alpha=25^\circ$ film effectiveness distribution resembled the experimental result in BR=2.0 case, as for the other region, film effectiveness distribution expanded rather than the experimental result. Even when the turbulence intensity became high, the CFD result hardly changed.

Figure 10 shows the film effectiveness distribution of diffuser hole case obtained by CFD. In diffuser hole case, the film effectiveness near the cooling holes was also higher than the experimental result. However, as compared with cylindrical hole case, the region where film effectiveness was very high was small in BR=1.0 case. In BR=2.0 case as well as cylindrical hole case, the film effectiveness over the downstream region was overpredicted. The reduction of film effectiveness by increase in turbulence intensity was not seen by diffuser hole case.

Figure 11 shows a comparison of spanwise averaged film

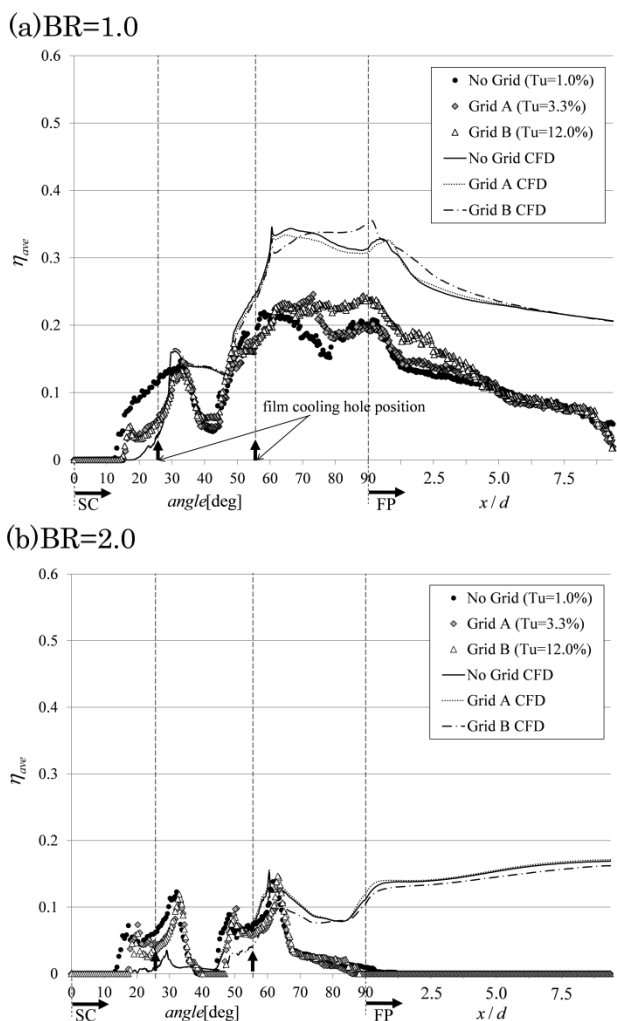


Fig.11 Spanwise-averaged film cooling effectiveness for cylindrical hole (a)BR=1.0 and (b)BR=2.0

effectiveness in cylindrical hole case. In the case of BR=1.0, when mainstream turbulence intensity was low (No Grid and Grid A), the spanwise averaged film effectiveness hardly changed. On the other hand, since film effectiveness distribution expanded in the spanwise direction, the spanwise averaged film effectiveness was slightly higher under Grid C case. The reduction of film effectiveness appeared faster than in the case of low mainstream turbulence intensity. Although the CFD result was qualitatively in agreement with the experimental result, there was a slight difference due to the effect of mainstream turbulence and CFD tended to overpredict. Since unsteady vortex structures was not predicted by CFD, it is considered that the reduction of spanwise averaged film effectiveness was hardly seen. As for the CFD result, in the case of BR=2.0, the difference from the experimental result became large remarkably in the downstream region from $\alpha=55^\circ$ cooling holes. The influence of mainstream turbulence intensity was small in the experiment.

Figure 12 shows a comparison of spanwise averaged film effectiveness in diffuser hole case. In the case of BR=1.0, unlike the case of cylindrical hole, the experimental result of diffuser hole case was decreased as the turbulence intensity became high in the downstream region from $\alpha=90^\circ$. However the change in CFD result due to the increasing of mainstream turbulence intensity was hardly seen as in cylindrical hole case. The CFD result of No Grid case was quantitatively close to the experimental result, but when the mainstream turbulence intensity became high, the effect of mainstream turbulence intensity was clearly identified compared with the CFD result. In the case of BR=2.0, when mainstream

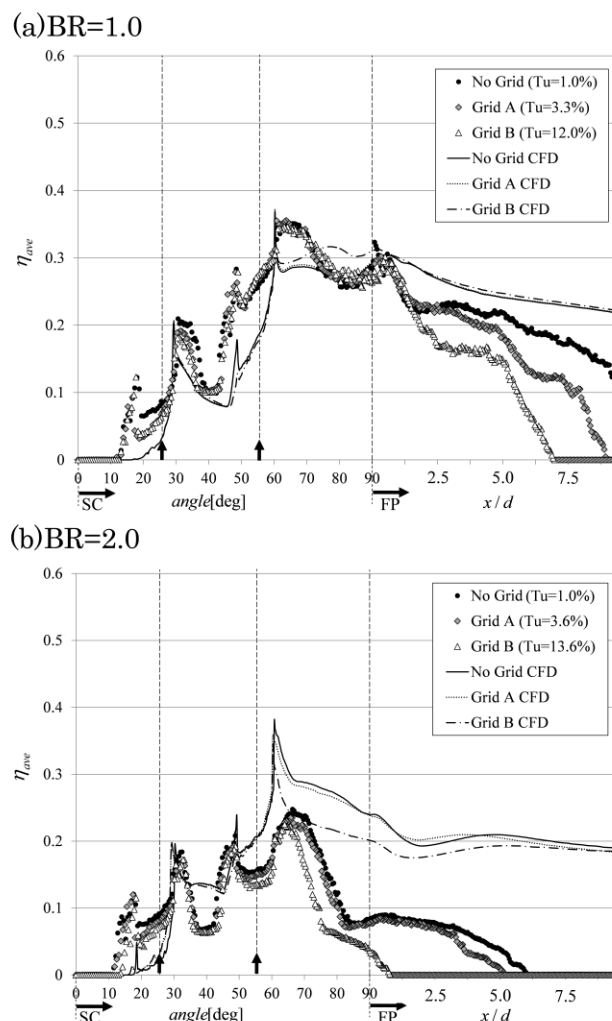


Fig.12 Spanwise-averaged film cooling effectiveness for diffuser hole (a)BR=1.0 and (b)BR=2.0

turbulence intensity was low (No Grid and Grid A), the experimental results were almost the same. On the other hand, the reduction of film effectiveness was observed at the downstream region from $\alpha=55^\circ$ cooling holes under the high mainstream turbulence intensity case. As for CFD result, by the increase of mainstream turbulence intensity, although spanwise averaged film effectiveness decreased in the $\alpha=55^\circ$ to 90° region, it was not remarkably decreased in flat plate region unlike the experiment case.

Figure 13 shows the distributions of measured and predicted local temperature on transverse plane normal to the model surface in cylindrical hole case. In the case of BR=0.5, the experimental results indicate that the mainstream and secondary air were mixed and the non-dimension temperature of Grid C case decreased compared with the case of No Grid. However, the influence of mainstream turbulence intensity was hardly seen in the attachment process of the secondary air. Although the non-dimensional temperature of the secondary air from $\alpha=25^\circ$ cooling holes was decreased, the diffusion to the spanwise direction was slightly large. In No Grid case, the CFD result was qualitatively in agreement with the experimental result. But, the CFD result became high compared with the experimental result. Furthermore, the reduction of the non-dimensional temperature according to the increase of mainstream turbulence intensity was not observed in the CFD result. In the case of BR=2.0, the experimental results show that the bulk of secondary air separated from the wall, indicating that the secondary air penetrates mainstream. Furthermore, when the non-dimensional temperature observed in the experiment from

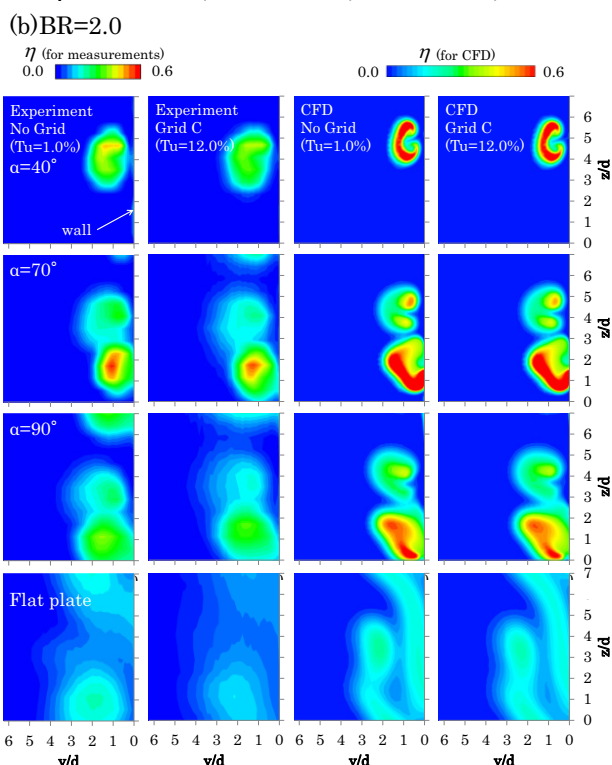
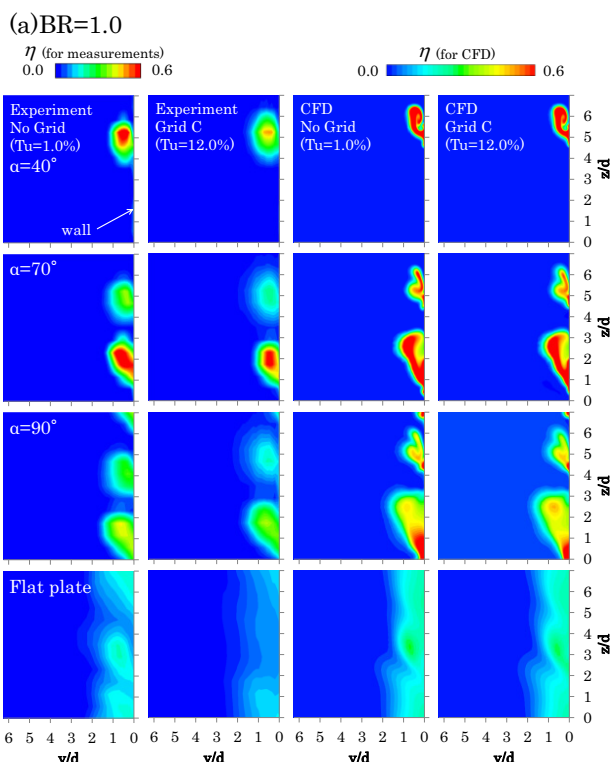


Fig.13 Local temperature on normal planes to model surfaces for cylindrical hole case (a)BR=1.0 and (b)BR=2.0

$\alpha = 25^\circ$ and $\alpha = 55^\circ$ cooling holes was compared, the secondary air from $\alpha = 55^\circ$ cooling holes attached to the model surface comparatively. The reduction of the non-dimensional temperature by the increase of mainstream turbulence intensity was similarly seen as in the case of BR=1.0. As for CFD result of BR=2.0 case, the non-dimensional temperature distribution was qualitatively in agreement on the plane normal to the semi-circular region, as for flat plate region, a large difference was seen between the experimental and CFD results in BR=2.0 case. Moreover, reduction of

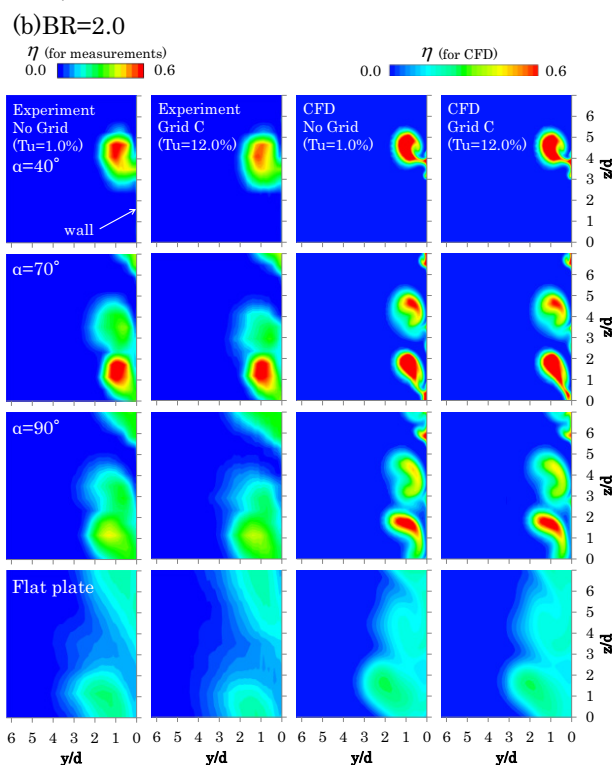
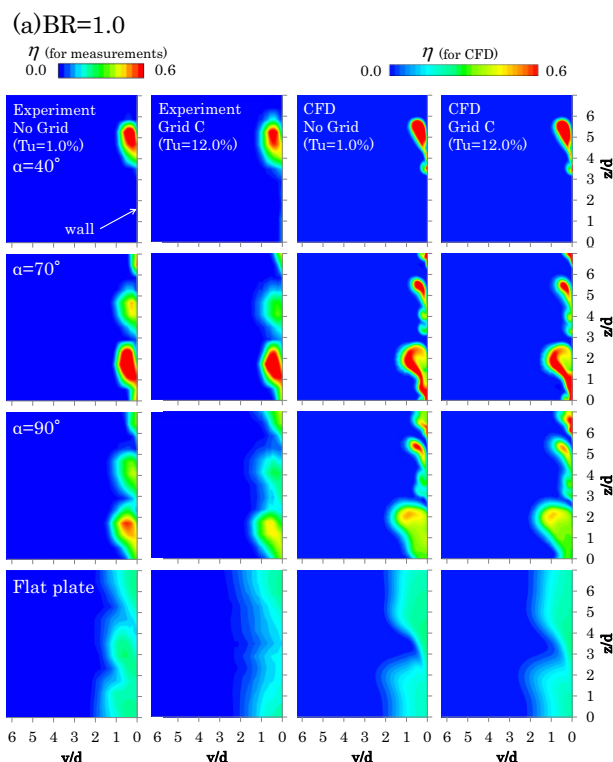


Fig.14 Local temperature on normal planes to model surfaces for diffuser hole case (a)BR=1.0 and (b)BR=2.0

non-dimensional temperature was not observed in the CFD result unlike the case of BR=1.0.

Figure 14 shows the distributions of measured and predicted local temperature on transverse plane normal to the model surface in diffuser hole case. As for the experimental result, in the case of BR=1.0, compared with the cylindrical hole case, the secondary air attached to the model surface. When the mainstream turbulence intensity became high, reduction of non-dimensional temperature was observed as in the result of cylindrical hole case. As for CFD result in BR=1.0 case, especially the bulk of secondary air from

$\alpha=25^\circ$ cooling hole differed from the experimental result. Reduction of the non-dimensional temperature by the increase of mainstream turbulence intensity was hardly seen as in the CFD result of cylindrical hole case. In the case of BR=2.0, the secondary air attached to the model surface as in BR=1.0 case. There are signs that the secondary air interfered within the $\alpha=70^\circ$ unlike the experimental result.

CONCLUSIONS

The influence of mainstream turbulence on leading edge film cooling was experimentally and numerically studied with two type of cooling holes. The main findings of the study are as follows.

In cylindrical hole case, under low BR, mainstream turbulence acted on the mixture of mainstream and secondary air, and the diffusivity of the secondary air which ejected from $\alpha=25^\circ$ cooling holes was improved. But it promoted the reduction of secondary air temperature. As a result, the spanwise averaged film effectiveness was decreased as the turbulence intensity became high. On the other hand, although the reduction of secondary air temperature on normal planes to model surfaces was observed, the spanwise averaged film effectiveness was hardly seen in BR=2.0 case.

In diffuse hole case, since the momentum in the cooling hole exit was low compared with that of cylindrical hole, the secondary air attached to the model surface and its diffusion over the surface became prominent. Also in the case of diffuser hole, secondary air temperature on normal planes to model surfaces was decreased as the turbulence intensity became high. In this case, the mainstream turbulence enhanced mixing of mainstream and secondary air in the streamwise and spanwise direction, and reduced the spanwise averaged film effectiveness significantly.

For both hole geometry cases the experimental result were reasonably in agreement with the CFD results in low BR. However the difference between the experimental result and CFD result became larger in high BR. Furthermore, in diffuser hole case, the effect of mainstream turbulence was hardly seen in CFD result. This is because it was not able to predict instability originated unsteady flow structure by CFD result using RANS.

ACKNOWLEDGMENT

The authors express their thanks to the Society of Japanese Aerospace Companies (SJAC), which give them an opportunity to conduct this research.

REFERENCES

- [1] Okita, Y., 2011, "Turbine Airfoil", Japanese Patent Application No.2011-085580
- [2] Mehendale, A.B., Han, J.C., 1992. "Influence of high mainstream turbulence on leading edge film cooling heat transfer" *ASME Journal of Turbomachinery*, Vol. 114, pp. 707-715
- [3] Ekkad, S.V., Du, H., Han, J.C., 1995. "Local heat transfer coefficient and film effectiveness distributions on a cylindrical leading edge model using a transient liquid crystal image method" *ASME Winter Annual Meeting, San Francisco, CA*.
- [4] Rozati, A., Tafti, D.K., 2007. "Large Eddy Simulation of leading edge film cooling part I : Computational domain and effect pipe inlet condition" *ASME Turbo Expo 2007, GT2007-27689*
- [5] Rozati, A., Tafti, D.K., 2007. "Large Eddy Simulation of leading edge film cooling part II : Heat transfer and effect of blowing ratio" *ASME Turbo Expo 2007, GT2007-27690*
- [6] Saumweber, C., Schulz, A., Witting, S., 2003. "Free-Stream turbulence effects on film cooling with shaped holes" *ASME Journal of Turbomachinery*, Vol. 125, pp. 65-73
- [7] Takahashi, T., Funazaki, K., Salleh, H.B., Sakai, E., Watanabe, K., 2010. "Assessment of URANS and DES for prediction of leading edge film cooling" *ASME Turbo Expo 2010, GT2010-22325*
- [8] Kim, Y.J., Kim, S.M., 2004. "Influence of shaped injection holes on turbine blade leading edge film cooling" *ASME*

Journal of Heat and mass transfer, Vol. 47, pp. 245-256

- [9] Reiss, H., Bolcs, A., 2000. "Experimental study of showerhead cooling on a cylinder comparing several configurations using cylindrical and shaped holes" *ASME Journal of Turbomachinery*, Vol. 122, pp. 161-169
- [10] York, W.D., Leylek, J.H., 2003. "Leading-edge film-cooling physics-Part III: Diffused hole effectiveness" *ASME Journal of Turbomachinery*, Vol. 125, pp. 252-259
- [11] Kim, Y. W., Downs, J.P., Coechting, F.O., Abdel-Messeh, W., Steuber, G. D. And Tanrikut, S., "A Summary of the Cooled Turbine Blade Tip Heat Transfer and Film Effectiveness Investigations Performed by Dr. D.E. Metzger," *ASME Trans., Journal of Turbomachinery*, Vol. 117, pp. 1-10